Available online at www.sciencedirect.com
ScienceDirect
Journal of Asian Earth Sciences 33 (2008) 139–154
Journal of Asian Earth Sciences
www.elsevier.com/locate/jaes

Dolerites of the Woodlark Basin (Papuan Peninsula, New Guinea): A geochemical record of the influence of a neighbouring subduction zone

Véronique Gardien [a,*], Christophe Lécuyer [a,1], Jean-François Moyen [b]

[a] UMR CNRS 5125 PEPS, Université Lyon1, 2 Rue Raphaël Dubois, Bat. Géode R5, 69622 Villeurbanne, France
[b] Department of Geology, University of Stellenbosch, Private Bag X17602 Matieland, South Africa

Received 8 March 2007; received in revised form 12 November 2007; accepted 18 December 2007

Abstract

The Moresby Seamount located in the Woodlark Basin is a fragment of oceanic crust (dolerites and gabbros) generated 66.4 ± 1.5 My ago before being obducted during the Eocene on the Australian margin. Since 8 My, the motion of a normal fault related to the opening of the Woodlark Basin is responsible for the unroofing of the Moresby seamount. The latter was sampled during the ODP campaign Leg 180 in 1998. Geochemical compositions of dolerites can be explained by a process of fractional crystallization in which the magnesian spinel was involved. Therefore fractionation processes took place at relatively high pressure (>1 GPa), most likely during the upward migration of deep magmas throughout the mantle. The Fe-rich gabbros, more differentiated than the dolerites, could have derived from an early differentiated magma evolving in the crust at relatively low pressures. The trace element content of dolerites indicates that their source was a depleted oceanic mantle slightly influenced by arc-related magmas. This study suggests that the ophiolites fragment of the Moresby seamount was created in the vicinity of a subduction zone; this model being in agreement with the regional tectonic setting of SE Asian since the Cainozoic.

Keywords: Woodlark basin; Leg 180; Dolerites

Contents

* Corresponding author.
E-mail address: vgardien@univ-lyon1.fr (V. Gardien).
[1] Institut Universitaire de France.

1367-9120/$ - see front matter © 2007 Elsevier Ltd. All rights reserved.
doi:10.1016/j.jseaes.2007.12.003

1. Introduction

The petrology and geochemistry of ophiolitic rocks commonly lead to discuss whether they reflect the composition of an oceanic mantle source potentially contaminated or not by a neighbouring subducted plate or continental crust in a context of back-arc basin environment (Beccaluva et al., 2004). The role of subduction zones in the genesis of several Cainozoic South East Asia ophiolites has been largely evoked since the 1980s (Jenner, 1981; Davies and Jacques, 1984; Permana, 1998; Monnier et al., 1995, 1999, 2000; Omang and Barber, 1996; Yumul et al., 1997; Tamayo, 2004).

The ocean floor of the Cainozoic South East Asia basins was almost completely consumed at active subduction zones except some fragments obducted onto the northern Australian margin and now trapped in cratonic areas such as the Papuan Ultramafic Belt (PUB) (Davies, 1971; Monnier et al., 1999). Most of the ophiolites in this area display a geochemical signature typical of back-arc magmas onto the arc to fore-arc sequences (Jenner, 1981; Davies and Jacques, 1984; Permana, 1998; Monnier et al., 1995, 1999, 2000; Omang and Barber, 1996; Yumul et al., 1997; Tamayo, 2004) suggesting that they correspond to oceanic crusts generated in a supra-subduction zone (Monnier et al., 1999; Pubellier et al., 2004). These previous geochemical data have been used to restore the Cainozoic regional tectonic setting in SE Asia. Pubellier et al. (2004) concluded that during the Late Mesozoic to Palaeogene, similar tectonic settings developed in the same way along the northern margin of Australia that led to the opening of several basins.

The region of Papua New Guinea in SE Asia is nowadays affected by the subduction zones of the Solomon Sea Triple Junction and for the last 8 My, by extension associated with westward-propagating spreading that opened the Woodlark Basin. The Moresby Seamount, just ahead of the apex of spreading, is part of the continental lithosphere of Papua New Guinea affected by rifting. The continental rifting developed an asymmetric rift basin bounded on the south by a low angle detachment that forms the north slope of Moresby Seamount (Fig. 1).

During Ocean Drilling Program Leg 180 in 1998 in the Woodlark Basin, three holes (1109, 1117, and 1118) reached the crystalline basement of Moresby Seamount which is composed mostly of dolerites, gabbros and rare basalts (Fig. 2). Dolerites and gabbros were dated by U–Pb and Ar–Ar methods applied to zircons and plagioclases, respectively. They point to a crystallisation age of 66 Ma followed by cooling ages between 59 and 44 Ma related

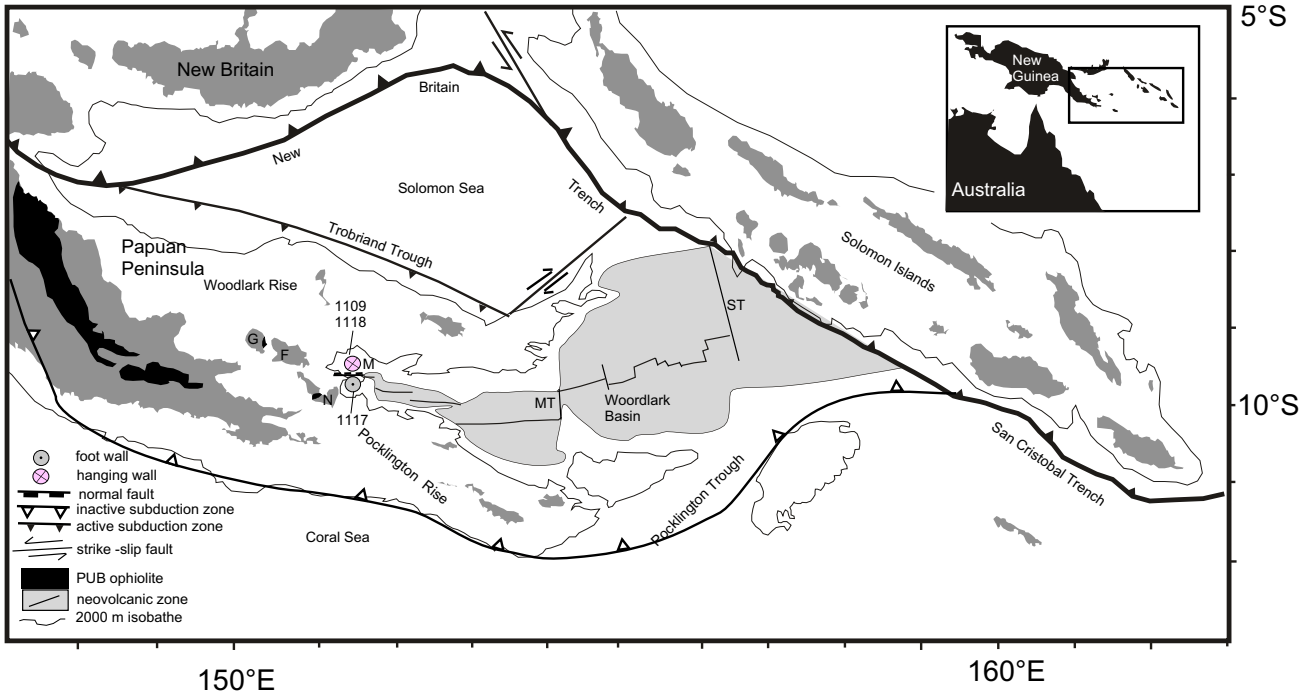

Fig. 1. Regional setting and tectonics of the Papua New Guinea region. MT, Moresby transform fault; ST, Simbo transform fault; M, Moresby seamount; G, Goodenough Island; F, Fergusson Island; N, Normanby Island. The top inset shows the geographic location of the study area (Modified from Gardien et al., 2001).

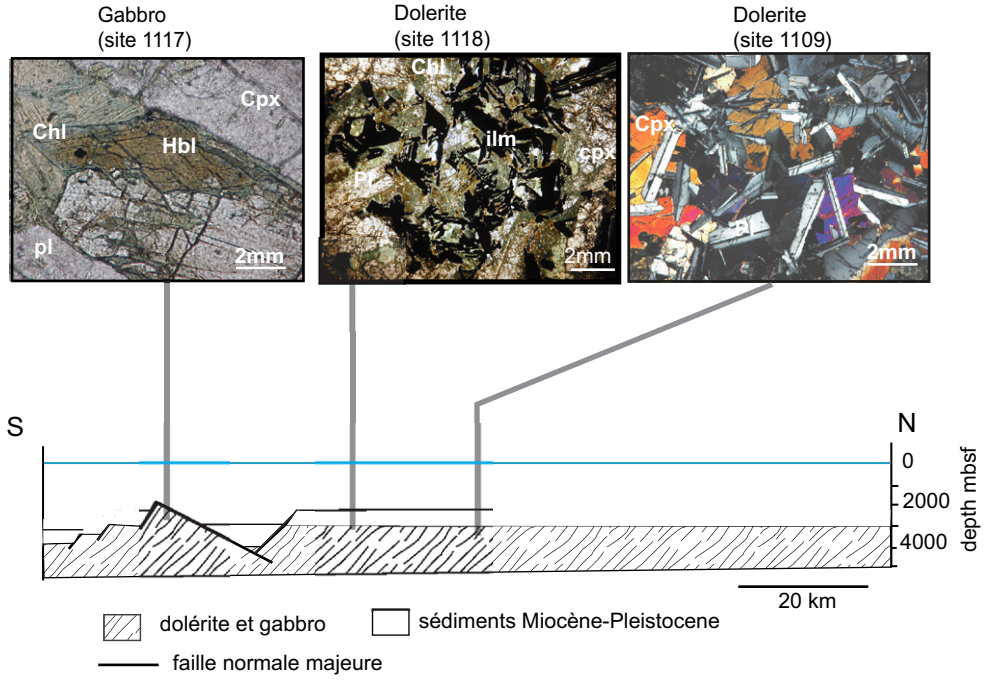

Fig. 2. Schematic cross section of the Moresby seamount in the Woodlark Basin showing the location of the three drilled sites. The mineralogy of gabbros and dolerites is illustrated by the photomicrographs.

to the obduction of the oceanic crust on the Australian Margin (Brooks and Tegner, 2001; Monteleone et al., 2001). These ages are contemporaneous with the various ophiolite-like fragments outcropping in the Woodlark area such as in the PUB that gave a Maastrichtian igneous crystallisation age (Smith and Davies, 1976; Belfort, 1976) and a final obduction age onto the Australian margin dated between 65 ± 0.7 and 57.2 ± 0.6 Ma (Lus et al., 2004). From previous geochemical data, Brooks and Tegner (2001) concluded that there was no direct connection between the PUB and the ophiolites drilled in the Woodlark Basin which might be expected from their geographical proximity (occurrences of PUB on the D'Entrecasteaux Islands, Fig. 1) and of their identical ages. Brooks and Tegner (2001) concluded for a possible similarity between the Ontong Java Large Igneous Province situated far to the East and on the opposite site of the Solomon Trench and the Leg 180 basement.

This study presents new major and trace element data in order to identify the parent magma and the processes that led to the petrogenesis of both Leg 180 dolerites and gabbros. Moreover this contribution discusses the possible affinities of these dolerites with other Woodlark Ophiolites and the Cainozoic SE Asia regional tectonic setting.

2. Petrology of the drilled rocks

During the ODP leg 180 (June 11–7 August 1998) in the Woodlark Basin, 11 sites (1108–1118) were drilled on the Moresby Seamount. Three of these sites (1109, 1117, and 1118) reached the crystalline basement. Sites 1109 and 1118 localised on the hanging wall of Moresby seamount produced predominantly dolerites, whereas the 1117 localised on the foot wall of the Moresby seamount detachment is made of gabbros (Fig. 2). Petrological and mineralogical descriptions, detailed in Gardien et al. (2001) are only summarized below.

2.1. Dolerites

Sites 1109 and 1118 are located in the hangingwall of the normal fault. Rare basalts occur along with the dominant dolerites. The dolerites contain iron oxides and have an ophitic texture with coarse grains made up of poekiloblastic clinopyroxenes containing radial plagioclase laths from 1 to 2 mm length. The basalts are made of a vitreous dark paste containing plagioclase microliths and spherules. The dolerites from site 1118 are characterized by a smaller grain-sized ophitic texture than those from site 1109 and they contain scarce serpentinized olivines, abundant clinopyroxenes, plagioclases, and dendritic iron oxides.

2.2. Gabbros

The site 1117 is located in the footwall of the normal fault. The rocks drilled in this site are quartz gabbros composed of plagioclases and interstitial pyroxenes associated with xenomorphic quartz and dendritic ilmenites. The textures of the rocks vary from a granular texture with fine grains (0.5–1 cm) at the base of the borehole where the gabbros are not deformed to a mylonitic texture at the top of the hole at the vicinity of the fault zone. This textural

Table 1A
Major and trace element analyses of gabbros from site 1117 (A) and dolerites from sites 1118 and 1109 (B, C, D, and E) that were drilled during Leg 180

Site	1117A	1117A	1117A	1117A	1117A	1117A	1117A
Core	11R-1	11R-1	11R-1	12R-1	12R-1	13R-1	14R-1
SiO_2	47.94	50.51	47.31	49.29	48.97	49.95	53.11
Al_2O_3	12.79	12.41	12.34	11.65	13.60	13.70	13.43
Fe_2O_3	17.84	19.33	18.23	21.6	14.52	12.00	13.53
MgO	4.89	4.33	4.90	4.37	6.05	6.03	5.82
CaO	8.48	8.43	8.08	8.71	9.12	10.74	10.24
Na_2O	4.37	2.83	5.39	1.95	3.58	4.07	2.77
K_2O	0.25	0.17	0.09	0.15	0.18	0.30	0.23
TiO_2	2.21	2.53	2.38	2.95	1.48	1.34	1.57
P_2O_5	0.21	0.19	0.20	0.17	0.10	0.11	0.11
MnO	0.25	0.27	0.26	0.27	0.23	0.23	0.24
H_2O	1.89	<L.D.	1.9	<L.D.	2.44	1.78	<L.D.
Sum	101.12	101	101.08	101.11	100.27	100.25	101.05
Al_2O_3/MgO	2.62	2.87	2.52	2.67	2.25	2.27	2.31
Sr/MgO	18.81	20.55	14.49	22.43	16.03	19.90	20.10
Fe_2O_3/TiO_2	8.07	7.64	7.66	7.32	9.81	8.96	8.62
Al_2O_3/Zr	0.11	0.12	0.10	0.14	0.19	0.20	0.19
TiO_2/Zr	0.02	0.03	0.02	0.04	0.02	0.02	0.02
Sc	38	<L.D.	41	<L.D.	40	39	<L.D.
V	448	502	482	813	362	340	387
Cr	1	<L.D.	1	<L.D.	3	8	<L.D.
Co	52	<L.D.	54	<L.D.	47	38	<L.D.
Ni	32	36	29	40	35	36	40
Cu	95	125	132	299	163	5	235
Rb	4.1	3	1.5	3	2.8	5.1	4
Sr	92	89	71	98	97	120	117
Ba	32	0	14	0	33	34	1
Zr	120	101	125	84	72	69	69
Nb	7	10	8.6	8	5.2	4.8	6
Y	46	35	45	30	29	28	24
Ce	<L.D.	<L.D.	<L.D.	<L.D.	<L.D.	<L.D.	5.5

Oxides are given in wt% and trace elements in ppm. The composition of the model mantle proposed by the GERM project for melting rates higher than 5% (http://earthref.org/GERM/) is mentioned in Table 1D and 1E.

variation is accompanied by a change in the mineralogy with the occurrence of green hornblende and chlorite in the fault zone (Fig. 2). The gabbros are overlain by argillaceous rocks interpreted as a fault gauge (Taylor et al., 1999).

3. Analytical techniques

3.1. Whole rock major and trace element chemistry

Forty-two samples from ODP sites 1109, 1117, and 1118 have been analyzed for major element contents and a subset of 22 samples has also been analyzed for trace element (Table 1), including Rare Earth Elements. Analyses were performed at the Centre de Recherches Pétrographiques et Géochimiques, Nancy, France, by using an ICP-OES Thermo Electron IRIS Advantage™ for major elements and an ICP-MS Perkin-Elmer Elan 6000™ for trace elements. The analytical procedures are described in details in Carignan et al. (2001). Samples were finely ground in an agate mortar before acid dissolution. Loss on ignition

Table 1B

Site	1118A	1118A	1118A	1118A	1118A	1118A	1118A	1118A	1118A	1118A	1118A	1118A	1118A	1118A
Core	69R-2	70R-1	70R-3	71R-1	72R-1	73R-1	74R-1	74R-2	76R-1	76R-1	76R-1	76R-2	76R-2	76R-2
SiO_2	48.78	47.56	47.72	47.08	51.27	47.48	47.53	46.49	43.41	51.83	48.40	51.99	47.86	49.89	46.99	48.18	50.44	47.97	51.55
Al_2O_3	16.09	12.52	14.45	14.70	13.55	14.53	12.49	14.08	14.56	13.17	13.05	12.85	13.10	13.37	13.67	13.80	14.33	13.49	13.89
Fe_2O_3	14.62	14.77	11.44	11.30	14.91	11.60	14.52	11.69	9.77	15.32	13.85	15.45	13.06	13.25	12.16	12.47	12.54	12.85	13.23
MgO	7.48	5.96	7.23	7.06	5.91	7.18	6.21	6.17	5.76	5.92	6.93	5.55	7.48	3.49	6.92	6.81	6.31	7.42	6.81
CaO	9.29	8.68	11.54	11.77	9.79	11.62	9.08	13.34	15.76	9.60	10.59	8.79	9.86	13.55	11.36	10.27	12.13	10.49	10.85
Na_2O	1.97	4.06	3.77	2.87	3.73	2.63	3.88	3.36	2.33	3.06	3.03	3.62	3.37	3.99	5.14	4.59	2.32	2.99	2.58
K_2O	0.15	0.21	0.15	0.13	0.19	0.13	0.21	0.15	0.15	0.45	0.11	0.23	0.21	0.53	0.40	0.36	0.34	0.26	0.21
TiO_2	1.87	1.80	1.48	1.51	1.83	1.47	1.70	1.49	1.45	1.74	1.56	1.78	1.41	1.79	1.51	1.42	1.59	1.44	1.48
P_2O_5	0.15	0.13	0.12	0.13	0.14	0.12	0.13	0.13	0.13	0.13	0.12	0.15	0.10	0.19	0.14	0.13	0.12	0.11	0.11
MnO	0.13	0.20	0.30	0.36	0.23	0.47	0.27	0.48	0.46	0.25	0.20	0.25	0.22	0.45	0.27	0.25	0.29	0.21	0.22
H_2O	<L.D.	2.97	3.27	4.16	<L.D.	3.00	3.16	3.57	6.49	<L.D.	1.54	<L.D.	2.18	<L.D.	2.71	2.45	<L.D.	2.11	<L.D.
Sum	100.53	98.86	101.47	101.07	101.55	100.23	99.18	100.95	100.27	101.47	99.38	100.66	98.85	100.50	101.27	100.73	100.41	99.34	100.93
Al_2O_3/MgO	2.15	2.10	2.00	2.08	2.29	2.02	2.01	2.28	2.53	2.22	1.88	2.32	1.75	3.83	1.98	2.03	2.27	1.82	2.04
Fe_2O_3/TiO_2	7.82	8.21	7.73	7.48	8.15	7.89	8.54	7.85	6.74	8.80	8.88	8.68	9.26	7.40	8.05	8.78	7.89	8.92	8.94

Table 1C

1118A	70R-1W,112	70R-3W,107	73R-1W,27–51	74R-2W,22–39	76R-2W,13–23	76R-2,45–53	74R-2,51–69
Cr	60.04	194.50	49.51	96.94	177.10	203.00	110.00
Ge	1.64	1.67	1.70	1.69	1.69	< L.D.	< L.D.
In	0.08	0.07	0.08	0.09	0.07	< L.D.	< L.D.
Sn	0.55	0.85	0.70	0.74	0.65	< L.D.	< L.D.
Ta	0.37	0.30	0.36	0.32	0.31	< L.D.	< L.D.
Tb	0.76	0.67	0.78	0.71	0.67	0.71	0.75
Tm	0.45	0.39	0.47	0.42	0.39	0.42	0.44
U	0.10	0.21	0.11	0.10	0.10	0.10	0.10
Zn	78.48	102.50	113.60	111.80	98.24	< L.D.	< L.D.
V	384.30	357.40	395.70	377.80	345.10	347.00	368.00
Co	46.42	51.95	53.95	50.66	50.49	51.00	52.00
Ni	54.05	81.71	55.46	70.26	77.21	85.00	75.00
Cu	35.25	165.40	201.50	189.90	168.90	< L.D.	< L.D.
Ga	18.22	18.54	19.26	18.31	18.20	17.10	22.50
Rb	2.55	1.79	2.69	1.04	2.10	2.60	1.00
Sr	159.20	149.40	188.50	122.70	144.00	154.00	141.00
Y	28.89	25.15	31.89	26.78	25.48	27.80	29.60
Zr	86.29	76.80	93.50	78.37	74.17	78.00	81.50
Nb	4.26	3.69	4.52	3.98	3.66	4.53	4.68
Ba	40.37	21.96	104.40	29.20	48.74	48.70	29.70
La	4.77	4.17	5.09	4.48	4.18	4.37	4.50
Ce	12.86	11.37	13.70	11.92	11.27	11.60	12.13
Pr	2.01	1.80	2.16	1.85	1.78	1.81	1.91
Nd	10.26	9.26	10.92	9.27	9.21	9.28	9.77
Sm	3.37	3.03	3.55	3.09	3.03	3.08	3.25
Eu	1.23	1.17	1.32	1.17	1.15	1.17	1.20
Gd	4.25	3.77	4.49	3.92	3.81	4.23	4.20
Dy	4.90	4.32	5.11	4.56	4.34	4.62	4.81
Ho	1.03	0.91	1.08	0.96	0.92	0.98	1.03
Er	2.99	2.56	3.10	2.75	2.61	2.72	2.87
Yb	3.00	2.57	3.10	2.80	2.62	2.66	2.81
Lu	0.47	0.39	0.48	0.43	0.41	0.40	0.46
Hf	2.42	2.13	2.56	2.18	2.07	2.13	2.23
Pb	1.49	2.09	< L.D.	< L.D.	< L.D.	0.19	0.44
Th	0.46	0.35	0.42	0.36	0.35	0.38	0.39
Sr/MgO	26.71	21.16	30.35	17.71	25.41	19.41	22.61
Al_2O_3/Zr	0.15	0.19	0.13	0.17	0.16	0.18	0.18
TiO_2/Zr	0.02	0.02	0.02	0.02	0.02	0.02	0.02

(L.O.I.) was determined by gravimetry after roasting whole rocks at 1000 °C over 4 h. The analytical error is in the range 1–5% for major elements, if their concentrations exceed 1 wt% and 2–10% for element concentrations below 1 wt%. Typical detection limits were between 0.001% (MnO) and 0.07% (Na_2O) for major elements; and between 0.005 ppm (Tm, Lu, Yb) and 8 ppm (Zn) for trace elements.

3.2. Calculation of rock modal compositions and elemental fluxes

Modal composition of the bulk rocks were recalculated from the bulk rock major elements composition (Table 1) and the method involves the calculation of the rock modal compositions from the mineral chemistry (microprobe data published in Gardien et al., 2001), and bulk rock compositions (Table 1) by using a standard least-square method pioneered by Bryan et al. (1969).

The magmatic modal proportions were calculated by correcting the metamorphic modal proportions (Table 2) from the metamorphic reactions that took place between low grade amphibolite and greenschist facies. Clinopyroxene was replaced by both hornblende and chlorite, and plagioclase was either albitized or replaced by epidote and more or less zoïsite. The major Ti-bearing phase – ilmenite – remained stable in the studied gabbros and dolerites that did not suffer extensive alteration by seawater. In the most altered rocks, ilmenite was replaced by sphene. Only the rough amplitude and direction of elemental fluxes have been estimated to detect the most sensitive elements and therefore the less reliable petrogenetic indicators of partial melting or fractional crystallization. The elemental fluxes were obtained by computing the difference between the chemical compositions of measured altered rocks and "computed magmatic rocks".

4. Geochemical data

Bulk rock analyses of Woodlark gabbros and dolerites are listed in Table 1. Major element contents show significant

Table 1D

Site	1109D	1109D	1109D	1109D	1109D	1109D	1109D	1109D	1109D	1109D	1109D	1109D	1109D	1109D	Depleted
Core	46R-1	47R-3	47R-5	48R-2	48R-3	48R-3	49R-1	49R-2	49R-3	49R-3	50R-1	50R-1	51R-1	51R-1	51R-3	51R-4	51R-4	Mantle
SiO_2	51.20	51.32	49.57	48.06	48.23	51.21	46.77	50.73	47.1	46.96	51.13	46.98	51.51	47.03	47.8	47.12	51.49	44.9
Al_2O_3	14.50	14.61	13.99	13.73	14.32	14.51	13.55	15.54	14.81	14.41	14.82	14.03	14.80	14.52	14	14.53	15.38	4.28
Fe_2O_3	12.74	12.68	11.59	12.48	11.17	12.44	13.29	12.14	11.48	11.28	12.52	11.43	12.38	11.76	12.06	11.89	11.41	8.07
MgO	6.12	6.33	7.48	7.20	7.47	6.84	7.09	7.01	7.71	8.28	7.02	7.76	7.52	7.86	8.18	7.45	7.077	38.22
CaO	12.64	12.62	10.03	11.93	12.65	12.37	10.45	12.59	11.83	11.58	12.28	11.72	12.10	11.47	11.42	10.88	12.53	3.5
Na_2O	1.74	1.72	3.28	2.35	2.27	1.64	3.97	1.66	2.94	2.41	1.59	2.85	1.57	3.23	2.11	3.31	1.94	0.29
K_2O	0.12	0.08	1.85	0.31	0.09	0.11	0.51	0.10	0.1	0.09	0.09	0.13	0.11	0.13	0.11	0.27	0.16	60 (ppm)
TiO_2	1.44	1.41	1.36	1.41	1.19	1.33	1.52	1.31	1.26	1.25	1.31	1.26	1.33	1.26	1.27	1.34	1.43	798 (ppm)
P_2O_5	0.12	0.12	0.11	0.11	0.09	0.11	0.15	0.11	0.1	0.1	0.10	0.11	0.10	0.12	0.1	0.12	0.11	40.7 (ppm)
MnO	0.19	0.18	0.15	0.18	0.17	0.19	0.20	0.19	0.18	0.18	0.19	0.18	0.19	0.17	0.19	0.18	0.18	1045 (ppm)
H_2O	< L.D.	< L.D.	2.36	1.71	1.55	< L.D.	3	< L.D.	3.18	2.81	< L.D.	2.9	< L.D.	2.07	1.39	3.07	< L.D.	
Sum	100.79	101.045	101.77	99.47	99.2	100.745	100.5	101.36	100.69	99.35	101.02	99.35	101.58	99.62	98.63	100.16	101.71	99.56
Al_2O_3/MgO	2.37	2.31	1.87	1.91	1.92	2.12	1.91	2.22	1.92	1.74	2.11	1.81	1.97	1.85	1.71	1.95	2.17	
Fe_2O_3/TiO_2	8.85	9.02	8.52	8.85	9.39	9.35	8.74	9.27	9.11	9.02	9.59	9.07	9.31	9.33	9.50	8.87	7.98	

variations in both gabbros and dolerites, e.g., SiO_2 contents range from 47.3% to 53% in dolerites and from 43.4% to 52% in gabbros; CaO from 8.1% to 10.7% and from 8.7% to 15.8%, Na_2O from 1.9% to 5.4% and from 1.6% to 5.1%, Fe_2O_3 from 12 to 21.7% and from 9.8% to 15.5%, and MgO from 4.3% to 6.1% and from 3.5% to 8.3%. In contrast, Al_2O_3 contents are less varying with ranges from 11.7% to 13.7% in gabbros and from 12.5% to 15.5% in dolerites suggesting that some differentiation and/or alteration affected the samples.

Dolerites, assumed to represent magmatic liquids, have rather uniform incompatible trace element contents, e.g., Zr = 65–93 ppm, La = 3.2–5.1 ppm, and Yb = 2.2–3.1 ppm, contrasting with the large variability in U (0.07–0.25 ppm), Pb (0.2–2.1 ppm) and Ba (16–118 ppm) contents that could be related to alteration processes (Table 1). REE patterns are characterized by a slight LREE depletion ($(La/Sm)N = 0.83$ to 0.94) and HREE enrichment ($(Sm/Yb)N = 1.22$ to 1.31) relative to the primitive mantle (Sun and McDonough, 1989). Compatible elements such Cr and Ni vary significantly from 49 to 516 ppm and from 54 to 108 ppm.

5. Discussion

5.1. Oceanic metamorphism and elemental mobility

Variability in geochemical compositions of basalts and dolerites can result from variability in their modal compositions and mineral chemistry, thus reflecting for example processes of fractional crystallization. Large scattering in chemical compositions of these rocks can also result from alteration by seawater, leading to net elemental gain or loss. Elemental mobility during hydrothermal alteration must be identified in these rocks before any attempt to use their geochemical compositions as petrogenetic indicators.

Undeformed but metamorphosed gabbro 11R1 developed up to 14 wt% of chlorite, 8 wt% of epidote and 7 wt% of zoïsite while gabbro 13R1, close to a shear zone, is characterized by the occurrence of hornblende (about 10 wt% of pargasite) as a high-temperature metamorphic phase. This paragenesis suggests that gabbros were metamorphosed by a seawater-derived hydrothermal aqueous solution with oxidizing properties compatible with a relative shallow level in the crust. Dolerites are characterized by a more simple metamorphic paragenesis made of chlorite (from 10 to 19 wt%) and slightly albitized plagioclase.

Gabbros 11R1 and 13R1 from site 1117 have comparable reconstituted magmatic modes with about fifty–fifty clinopyroxene and plagioclase. Two types of gabbros can be distinguished (1) low Al_2O_3/MgO (2.3) and relatively high Fe_2O_3/TiO_2 (9.1) rocks, and (2) higher Al_2O_3/MgO (ca. 2.7) samples with lower Fe_2O_3/TiO_2 (7.7). These geochemical ratios reflect variations in the relative abundance of clinopyroxene and ilmenite, indicating the cumulative nature of these rocks.

Table 1E

1109D	47R-5W, 9–15	48R-2W, 87-10	49R-1W, 33–39	49R-3W, 120–125	151R-3W, 0–16	51R-3W, 40–47	51R-3W, 97-11	48R-2W, 40–80	Dep. Mantle
Cr	212.70	302.00	515.70	373.90	362.70	275.20	311.10	371.00	2500.00
Ge	1.78	1.74	1.52	1.55	1.62	1.23	1.63	< L.D.	1.00
In	0.10	0.08	0.09	0.07	0.08	0.06	0.07	< L.D.	12.20
Sn	0.63	1.17	0.77	0.57	0.73	0.71	1.11	< L.D.	0.10
Ta	0.26	0.26	0.27	0.21	0.25	0.20	0.25	< L.D.	13.80
Tb	0.69	0.68	0.65	0.58	0.65	0.51	0.64	0.70	0.08
Tm	0.39	0.39	0.38	0.34	0.37	0.30	0.37	0.40	0.06
U	0.09	0.08	0.08	0.07	0.08	0.25	0.19	0.08	4.70
Zn	78.33	107.20	98.00	80.54	95.89	71.74	92.93	< L.D.	56.00
V	342.60	316.50	301.70	283.40	309.80	242.70	304.30	308.00	79.00
Co	48.93	49.63	50.06	48.62	52.79	39.13	49.18	49.00	106.00
Ni	64.08	78.65	82.83	102.30	108.10	80.95	82.93	83.00	1960.00
Cu	124.90	135.50	99.68	127.10	139.60	103.10	140.20	< L.D.	30.00
Ga	17.57	18.07	16.96	16.33	18.44	14.66	17.48	17.30	3.20
Rb	5.97	1.76	3.04	0.84	1.35	1.13	1.36	1.50	0.09
Sr	130.70	129.00	139.80	120.00	127.70	110.90	131.60	133.00	9.80
Y	25.68	25.72	24.83	22.02	24.53	20.13	24.71	27.50	4.07
Zr	74.34	75.90	75.67	64.84	71.58	55.08	72.22	75.90	7.94
Nb	3.12	3.23	3.18	2.69	2.93	2.30	2.97	3.74	210.00
Ba	117.60	20.88	32.44	16.13	19.83	15.96	18.74	20.00	1.20
La	3.98	4.03	3.94	3.23	3.68	3.21	3.80	3.92	0.23
Ce	10.94	10.83	10.78	9.07	10.02	8.23	10.32	10.63	0.77
Pr	1.77	1.73	1.73	1.45	1.62	1.32	1.65	1.71	0.13
Nd	9.14	8.92	8.89	7.64	8.49	6.89	8.67	8.81	0.71
Sm	3.04	3.01	2.96	2.52	2.79	2.28	2.78	3.00	0.27
Eu	1.19	1.20	1.14	1.02	1.10	0.91	1.11	1.18	0.11
Gd	3.87	3.74	3.63	3.27	3.58	2.95	3.59	4.12	0.39
Dy	4.40	4.38	4.23	3.74	4.10	3.33	4.15	4.47	0.53
Ho	0.92	0.94	0.89	0.78	0.87	0.70	0.87	0.95	0.12
Er	2.64	2.64	2.56	2.26	2.54	2.03	2.51	2.69	0.37
Yb	2.63	2.56	2.52	2.24	2.43	2.01	2.46	2.56	0.40
Lu	0.40	0.40	0.38	0.35	0.37	0.31	0.38	0.40	0.06
Hf	2.09	2.13	2.02	1.80	1.97	1.51	2.04	2.10	0.19
Pb	< L.D.	1.43	< L.D.	< L.D.	< L.D.	< L.D.	< L.D.	1.32	23.20
Th	0.30	0.30	0.30	0.26	0.28	0.23	0.29	0.32	13.70
Sr/MgO	17.47	17.92	19.72	15.56	15.61	17.66	14.11	17.7	
Al_2O_3/Zr	0.19	0.18	0.18	0.18	0.23	0.2	0.26	0.19	
TiO_2/Zr	0.02	0.02	0.02	0.02	0.02	0.02	0.02	0.02	

Dolerites from sites 1109 and 1118 have calculated magmatic modal compositions ranging from 50–57 wt% clinopyroxene, 40–43 wt% plagioclase and 3–7 wt% ilmenite. These rather narrow variations in the original magmatic modal compositions cannot explain alone the large chemical compositions observed in the resulting altered gabbros and dolerites. Indeed, the calculation of elemental fluxes in grams per 100 g of rock (Table 2) lead to identify the main chemical fluxes: (1) significant losses of Ca and Si by the rocks that can be related to the chloritization of clinopyroxene, (2) a small and rather uniform loss of Mg by the rocks, (3) various gains of Na during albitization of plagioclase, (4) large gains of Fe trapped in several Fe-rich phases such as hornblende, chlorite, and epidote, and (5) loss or gain of Al by the rocks depending on the extent of two competing metamorphic reactions that are the albitization of plagioclase (Al loss) and the chloritization of clinopyroxene (Al gain).

Moreover, the examination of chemical ratios (Table 1) suggests that REE, Zr and Ti were relative immobile during the processes of alteration of both gabbros and dolerites. In a general way, concentrations of alkali and calc-alkali elements have been largely modified through exchange with seawater. The more reliable element is Mg for which variations owing to alteration are of about ±0.5 wt%, which do not represent more than 20% of the total range observed in dolerites from both sites 1118 and 1109. The MgO content remains a very useful index for detecting and quantifying processes of fractional crystallization and should be preferred to the less robust Mg# index.

5.2. Magmatic evolution of the dolerites and gabbros

5.2.1. Dolerites of the hanging wall (sites 1109 and 1118)

The dolerites sampled from these two sites have similar geochemical compositions (Table 1). Their contents in Al_2O_3, Cr, Ni, and Ti have been reported as a function of MgO (Fig. 3). The resulting diagrams show well-defined trends except for Al_2O_3 whose contents have been disturbed by alteration processes. Variations in Ti, Ni, and

Table 2A
Modal compositions of a selection of gabbros and dolerites from Leg 180 showing fluxes of elements resulting from the alteration of the rocks by seawater

1117 Gabbro 13R1	Whole rock	Cpx	Ilm	Pg1	*mag Pg*	Chl	Hbl	Ep	Zo	"Fresh" rock	"Flux"
SiO_2	48.97	50.95	0.11	67.79	*55.72*	28.75	45.35	37.85	49.6	50.91	−1.94
Al_2O_3	13.6	1.803	2	20.91	*28.27*	16.32	7.25	21.51	20.09	14.86	−1.26
FeOt	14.52	14.14	68.74	0.31	*0.87*	33.19	18.5	15.05	2.66	10.16	4.36
MgO	6.05	14.87	0.07	0	*0.1*	10.73	12.75	0	0.44	6.89	−0.84
CaO	9.12	17.33	0.34	0.65	*11.23*	0.16	9.2	0	23.04	13.52	−4.40
Na_2O	3.58	0.27	0.04	10.99	*4.89*	0.07	2.36	23.18	0.04	2.54	1.04
K_2O	0.18	0	0	0.037	*0.08*	0	0.03	0	0.01	0.04	0.14
TiO_2	1.48	0.535	27.44	0	*0*	0.01	1.05	0	0.01	1.54	−0.06
H_2O	2	0	0	0	*0*	11.4	2	2.2	4	0.00	2.00
Sum	99.5	99.898	98.74	100.687	101.16	100.63	98.49	99.79	99.89	100.47	

1117 Gabbro 11R1	Whole rock	Cpx	Ilm	Pg1	*mag Pg*	Chl	Ep	Zo		"Fresh" rock	"Flux"
SiO_2	47.31	50.62	0.11	67.92	*55.72*	28.75	37.85	49.6		48.73	−1.42
Al_2O_3	12.34	2.3	2	20.41	*28.27*	16.32	21.51	20.09		14.01	−1.67
FeOt	18.23	12.53	68.74	0.09	*0.87*	33.19	15.05	2.66		11.93	6.30
MgO	4.9	14.42	0.07	0	*0.1*	10.73	0	0.44		6.76	−1.86
CaO	8.08	17.94	2.63	0.48	*11.23*	0.16	0	23.04		13.64	−5.56
Na_2O	5.39	0.28	0.082	11.46	*4.89*	0.07	23.18	0.04		2.35	3.04
K_2O	0.09	0	0.014	0.106	*0.08*	0	0	0.01		0.04	0.05
TiO_2	2.38	0.85	27.44	0	*0*	0.01	0	0.01		2.67	−0.29
H_2O	1.9	0	0	0	*0*	11.4	2.2	4		0.00	1.90
Sum	100.62	98.94	101.086	100.466	101.16	100.63	99.79	99.89		100.12	

Gabbro 1117 13R1					"Model"	Gabbro 1117 11R1					"Model"
Minerals	"Altered" mode	Minerals	"Fresh" mode	SiO_2	48.93	Minerals	"Altered" mode	"Fresh"	"Fresh" mode	SiO_2	47.33
Cpx	23			Al_2O_3	13.54	Cpx1	12.2			Al_2O_3	12.24
Ilm	4.7			FeOt	14.52	Cpx2	20	Cpx	46.5	FeOt	18.19
Pg	31.9	Cpx	46	MgO	6.02	Ilm	8.3	Ilm	8.3	MgO	4.86
Chl	12.5	Ilm	4.7	CaO	9.18	Pg	30	Pg	45.2	CaO	8.09
Hbl	10.5	Pg	49.3	Na_2O	3.8	Chl	14.3	Sum	100	Na_2O	5.45
Ep	11	Sum	100	K_2O	0.01	Ep	7.9			K_2O	0.03
Zo	6.4			TiO_2	1.47	Zo	7.3			TiO_2	2.48
Sum	100			H_2O	2.12	Sum	100			H_2O	2.13
MSWD = 0.183				Sum	99.59	MSWD = 0.167				Sum	100.80

(A) Gabbros from site 1117. (B) Dolerite from site 1118. (C) Dolerites from site 1109. "Fresh rock" corresponds to the calculated magmatic composition based on a linear combination of the magmatic compositions of relict minerals (Cpx, Ilm and *mag Pg*) and the reconstituted "fresh mode". The latter was obtained from the calculated "altered" mode corrected from the metamorphic reactions that were deduced from observations in thin sections. The "flux" means the elemental flux (in oxide grams per 100 g of rock) which was obtained by computing the difference between the calculated magmatic whole rock composition and the measured one. The "model" is the model whole rock composition corresponding to the calculated "altered" modal composition of the rock and that needs to be compared with the measured whole rock composition. When both compositions are very close, it means a high quality of the fit between the data and the model which is measured by a low value for the sum of squares of the residuals (MSWD). See the text for the mineral abbreviations and the explanation of the least-squares calculation method of modal compositions.

Table 2B

1118	Dolerite 72R1	Cpx	Ilm	Pg1	Pg2	Chl	"Fresh rock"	"Flux"	Modes			
SiO_2	47.48	51.58	0.56	57.59	56.83	30.48	50.64	−3.16	Minerals	"Altered" mode	Minerals	"Fresh" mode
Al_2O_3	14.53	2.26	3	26.86	28.17	14.86	13.06	1.47	Cpx	34.7	Cpx	50
FeOt	11.6	8.49	66.19	0.06	0.07	26.53	8.77	2.83	Pg	33.9	Pg1	33.9
MgO	7.18	16.61	0.08	0.68	0.74	13.65	8.61	−1.43	Pg2	9.3	Pg2	9.3
CaO	11.62	19.76	0.42	9.1	10.55	1.27	13.97	−2.35	Ilm	6.8	Ilm	6.8
Na_2O	2.63	0.27	0.08	6.56	3.34	0.04	2.67	−0.04	Chl	15.3		
K_2O	0.13	0	0	0.09	0.11	0	0.04	0.09	Sum	100	Sum	100
TiO_2	1.47	0.52	21.09	0	0	0.04	1.69	−0.22	MSWD = 0.695			
H_2O	3	0	0	0	0	13.1	0.00	3.00				
Sum	99.64	99.49	91.42	100.94	99.81	99.97	99.46					

Cr contents are compatible with processes of fractional crystallization involving clinopyroxene, plagioclase, ilmenite, and a Mg–bearing mineral that could be either olivine or Mg–spinel (Fig. 3). The geochemical composition of the 'model cumulate' required to describe the observed evolution between the most primitive (sample 49R-3W 80–83, hole 1109D, Table 1) and most differentiated dolerite samples (74R-1-107-110, hole 1118A, Table 1) has been esti-

Table 2C

1109 Dolerite 48R3	Whole rock	Cpx	Ilm	Pg	Chl	"Fresh" rock	"Flux"	Modes			
SiO_2	48.23	52.98	0.09	55.72	30.31	50.42	−2.19				
Al_2O_3	14.32	3.27	1	28.27	15.34	13.54	0.78	Minerals	"Altered" mode	Minerals	"Fresh" mode
FeOt	11.17	5.97	74.25	0.87	27.21	8.62	2.55	Cpx	40.3	Cpx	51.3
MgO	7.47	16.03	0.42	0.1	13.69	8.29	−0.82	Pg	41.7	Pg	41.7
CaO	12.65	20.33	0.01	11.23	1.72	15.11	−2.46	Ilm	7	Ilm	7
Na_2O	2.27	0.25	0	4.89	0.012	2.17	0.10	Chl	11		
K_2O	0.09	0	0.02	0.08	0	0.03	0.06	Sum	100	Sum	100
TiO_2	1.19	0.72	18.73	0	0.04	1.68	−0.49	MSWD = 0.444			
H_2O	1.55	0	0	0	11.4	0.00	1.55				
Sum	98.94	99.55	94.52	101.16	99.722	99.87					
1109 Dolerite 51R3	Whole rock	Cpx	Ilm	Plag	Chl	"Fresh" rock	"Flux"	Modes			
SiO_2	47.8	51.12	0.11	54.94	29.3	51.12	−3.32				
Al_2O_3	14	2.03	1	27.55	15.24	12.21	1.79	Minerals	"Altered" mode	Minerals	"Fresh" mode
FeOt	12.06	13.02	71.3	0.79	30.78	9.88	2.18	Cpx	42.4	Cpx	57
MgO	8.18	14.85	0.4	0.1	11.27	8.52	−0.34	Plag	40	Plag	40
CaO	11.42	17.5	0.01	10.79	1.64	14.29	−2.87	Ilm	3	Ilm	3
Na_2O	2.11	0.27	0	5.34	0.03	2.29	−0.18	Chl	14.6		
K_2O	0.11	0	0	0.05	0	0.02	0.09	Sum	100	Sum	100
TiO_2	1.27	0.78	23.56	0	0.07	1.15	0.12	MSWD = 0.293			
H_2O	1.39	0	0	0	11.5	0.00	1.39				
Sum	98.34	99.57	96.38	99.56	99.83	99.47					
1109 Dolerite 51R1	Whole rock	Cpx	Ilm	Plag	Chl	"Fresh" rock	"Flux"	Modes			
SiO_2	47.03	51.22	0.11	54.94	30.31	50.99	−3.96				
Al_2O_3	14.52	2.03	1	27.55	15.34	12.71	1.81	Minerals	"Altered" mode	Minerals	"Fresh" mode
FeOt	11.76	13.02	71.3	0.79	27.21	9.92	1.84	Cpx	38	Cpx	54.5
MgO	7.86	14.85	0.4	0.1	13.69	8.15	−0.29	Plag	42	Plag	42
CaO	11.47	17.5	0	10.79	1.72	14.07	−2.60	Ilm	3.5	Ilm	3.5
Na_2O	3.23	0.27	0	5.34	0.12	2.39	0.84	Chl	16.5		
K_2O	0.13	0	0	0.05	0	0.02	0.11	Sum	100	Sum	100
TiO_2	1.26	0.78	23.56	0	0.04	1.25	0.01	MSWD = 0.398			
H_2O	2.07	0	0	0	11.4	0.00	2.07				
Sum	99.33	99.67	96.37	99.56	99.83	99.51					
110 Basalt 51R49	Whole rock	Cpx	Ilm	Pg	Chl	"Fresh" rock	"Flux"	Modes			
SiO_2	47.12	52.66	0.08	54.94	27.99	51.20	−4.08				
Al_2O_3	14.53	2.65	1	27.55	16.1	13.03	1.50	Minerals	"Altered" mode	Minerals	"Fresh" mode
FeOt	11.89	6.44	74.25	0.79	31.87	7.19	4.70	Cpx	34.7	Cpx	53.4
MgO	7.45	17.26	0.42	0.1	11.25	9.28	−1.83	Plag	42	Plag	42
CaO	10.88	19.67	0.01	10.79	1.27	15.04	−4.16	Ilm	4.6	Ilm	4.6
Na_2O	3.31	0.24	0	5.34	0.04	2.37	0.94	Chl	18.7		
K_2O	0.27	0	0.02	0.05	0	0.02	0.25	Sum	100	Sum	100
TiO_2	1.34	0.49	18.73	0	0.13	1.12	0.22	MSWD = 0.861			
H_2O	3.07	0	0	0	11	0.00	3.07				
Sum	99.86	99.41	94.51	99.56	99.65	99.25					

mated using major and trace element mass balance calculations (Table 3).

For each major oxide, the difference between the compositions of the differentiated "observed" magma and that of the "model" magma is computed (Table 2). The sum of squares of errors is used as an indicator of the quality of the model (Martin, 1985; Moyen et al., 2001). None of the calculated models gives a satisfactory solution considering that the sum of squares of errors is always comprised between 20 and 30. However, an acceptable model output is the fractionation of 30 to 40 wt% of a cumulate composed mostly of clinopyroxene (about 65 wt%), plagioclase (20 wt%) and oxides (15 wt%) which are magnesian spinel, magnetite, and ilmenite. Even though all these minerals are observed in the dolerites, it cannot be excluded that small amounts of olivine can be involved in the fractionation process.

Contrasting with major elements, the model gives better results using trace elements (Table 3). The composition of the differentiated liquid, recalculated on the basis of both the cumulative mineralogy described above and the partition coefficients given by Rollinson (1993), is similar to the "differentiated" sample (74R-1-107-110, hole 1118A). Table 1 shows that the geochemical differentiation of the magma requires fractionation of minerals that have a Mg/Fe ratio higher than 1.5 and silica content lower than 46 wt%. Neither the clinopyroxene nor the olivine are good candidates because they are too silica-rich (51 wt%) and not magnesian enough (Mg/Fe = 4.72), respectively. Only the magnesian spinel can

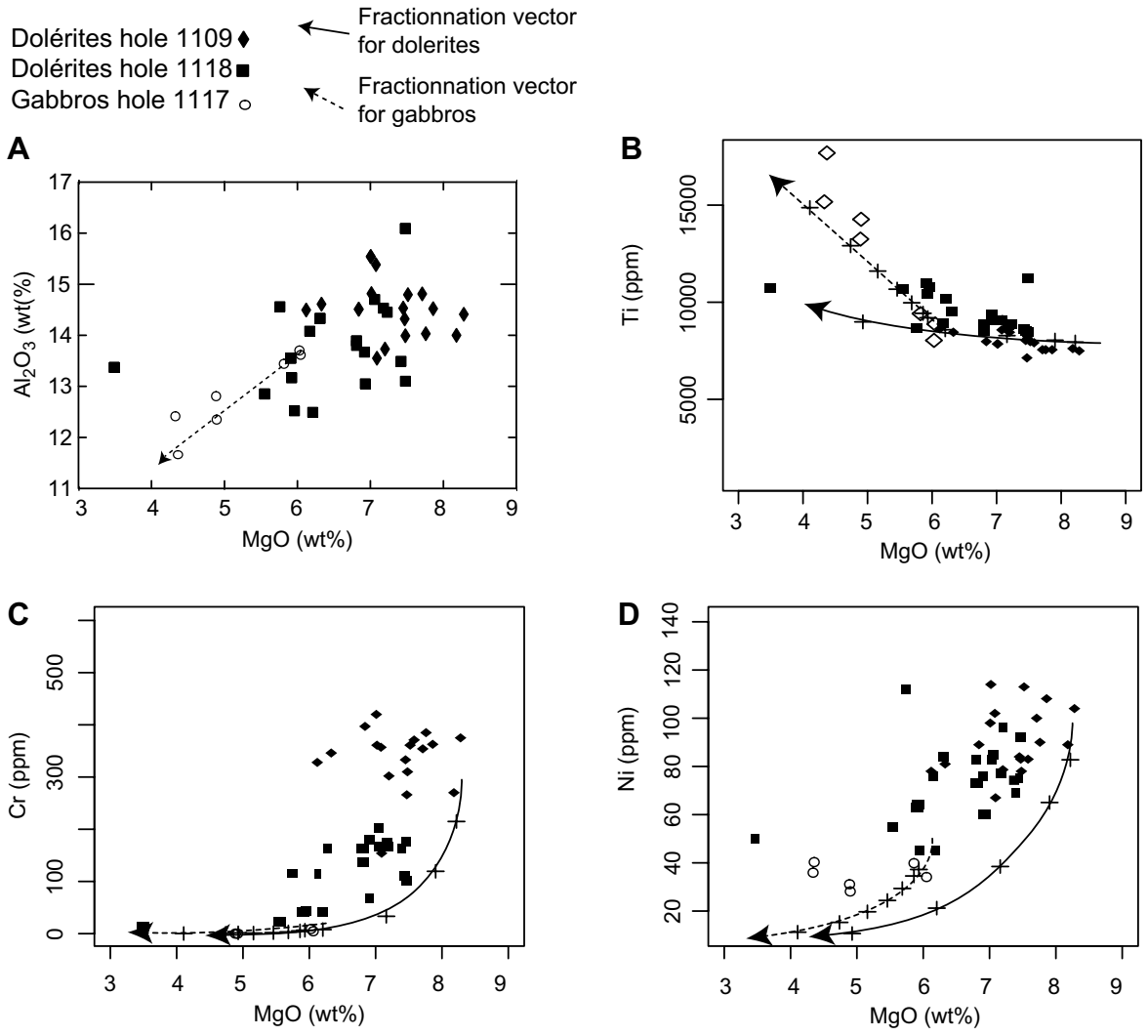

Fig. 3. Variations in Al_2O_3 (A), Ti (B), Cr (C), and Ni (D) contents reported against MgO contents of Woodlark dolerites and gabbros. Fractionation models (B, C, and D) have been computed for dolerites (1) and gabbros (2). (1) Crosses correspond to 5%, 10%, 20%, 30%, and 40% of fractional crystallization of the following minerals: 19% plagioclase, 15% Fe–Ti–Mg oxides and 66% clinopyroxene; (Table 3). (2) Crosses correspond to 5%, 10%, 20%, 30%, 40%, 50%, and 60% of fractionation of the following minerals: 52% feldspar, 8% spinel and 40% clinopyroxene. Dolerites from site 1109: filled diamonds. Dolerites from site 1118: filled squares. Gabbros from 1117: open circles. Black arrow: fractionation vector for dolerites; dashed black arrow: fractionation vector for the gabbros.

match the required chemical composition. The geochemical composition of dolerites can be thus explained by a process of fractional crystallization in which the magnesian spinel was present.

5.2.2. Gabbros of the "footwall", site 1117

The gabbros have higher Fe, Nb, Y and lower MgO, Ni, and Cr contents than dolerites, indicating their more differentiated geochemical character (Table 1 and Fig. 3). Fractional crystallization could partly explain the geochemical evolution of gabbros, involving plagioclase, clinopyroxene and ilmenite (Fig. 3), thus corresponding to the low pressure eutectic of the basaltic system (Green and Ringwood, 1967). The gabbros, more differentiated than dolerites, most likely evolved from an already differentiated magma stored at a shallow level in the oceanic crust. This hypothesis is supported by the chemistry of clinopyroxene. Indeed, partition between Al^{IV} and Al^{VI}, deduced from their computed structural formulae, suggests that clinopyroxene in dolerites crystallized in the medium pressure field (0.8 GPa) whereas those from gabbros crystallized in the low pressure field (0.4 GPa) (Gardien et al., 2001). This result is at variance with the fractionation of magnesian spinel that took place at relative high pressures (>1 GPa; Green and Ringwood, 1967) during the upward migration of the parent magma of dolerites throughout the mantle.

5.3. Mantle source and the genesis of dolerite parental magma

As pointed out by Brooks and Tegner (2001), a MORB-normalized diagram shows a slight enrichment in the most immobile incompatible elements that are K, Ba, Th, and Ta (Fig. 4A). However, some LILE elements

Table 3
A possible model based on a mass balance calculation describes the process of fractional crystallization of dolerites

	Initial liquid	Minerals						Differentiated liquid		Difference
		(Composition after Gardien et al., 2001)					Cumulate	Calculated	Sample	
	49R-3W-80–87	Pg	Mg–Sp	Mt	Ilm	Cpx			74R-1W-107–110	
SiO2	46.96	55.72	–	0.26	0.56	51	44.39	*48.67*	51.83	−3.16
Al2O3	14.41	28.27	65.4	0.2	3	3.23	15.61	*13.61*	13.17	0.44
Fe2O3	11.28	0.97	12	99.54	73.54	7.07	8.15	*13.37*	15.32	−1.95
MgO	8.28	0.1	22	0.01	0.08	16.81	13.86	*4.56*	5.92	−1.36
CaO	11.58	11.23	–	–	0.42	20.12	15.48	*8.98*	9.6	−0.62
Na2O	2.41	4.89	–	–	0.08	0.25	1.1	*3.29*	3.06	–
K2O	0.09	0.08	–	–	–	–	0.02	*0.14*	0.45	–
TiO2	1.25	–	0.13	–	21.09	0.73	1.02	*1.4*	1.74	−0.34
P2O5	0.1	–	–	–	–	–	0	*0.17*	0.13	0
Mg/Fe	1.46	0.21	3.64	0	0	4.72	3.38	*0.68*	0.77	
	Mineral % in cumulate	19%	12.30%	0%	2.50%	66.30%	Mass prop. of cumulate: 0.4			Sum of squared diff: 16.33
Zr	70	0.25	0.1	1.00E-05	1.00E-05	0.35	0.3	*101*	86	15
Y	24	0.6	0.15	1.00E-05	1.00E-05	0.3	0.3	*34*	27	7
Nb	3	0.025	0.2	1.00E-05	1.00E-05	0.3	0.2	*5*	7	−2
Sr	121	2	1.00E-05	1.00E-05	1.00E-05	0.12	0.5	*159*	146	13
Ba	19	0.26	1.00E-05	1.00E-05	1.00E-05	0.026	0.1	*31*	3	28
Rb	2	0.06	1.00E-05	1.00E-05	1.00E-05	0.03	0	*3*	7	−4
V	277	0.01	0.2	8.6	8.3	0.8	0.8	*313*	351	−38
Ni	104	0.1	25	8.6	4.5	3.4	5.5	*11*	64	−53
Cr	375	0.01	50	8	6	8.4	11.9	*1*	41	−40
Co	47	0.03	5	9.5	5.9	1,5	1.8	*32*	nd	

Clinopyroxene and magnesian spinel played a major role in the 40 wt% fractionation of a cumulate that mostly explain how the primitive liquid (column "Initial liquid") evolves towards a "model" differentiated liquid (in italic column "Initial liquid") for which its composition tends to approach the most differentiated dolerite observed (sample column in "Differentiated liquid"). Differences, quantified by the mean square weight deviation (MSWD) between these two latter geochemical compositions are reported in the rightmost column (column "Difference") except for the alkali elements that were mobile during alteration processes. In the lower part of the table, the effect of fractionation crystallization on trace element contents is also reported.

such as K, Rb, and Ba, showing a large scattering in their relative abundance, are suspected of high mobility during the alteration of dolerites. They have been therefore excluded from the multi-element diagram in Fig. 4B, thus revealing the homogenous geochemical signature of Leg 180 dolerites. This relative weak enrichment in the most incompatible elements could be related either to a discrete influence of a deep-seated component (OIB or EMORB) or an adjacent subduction zone. On one hand, Brooks and Tegner (2001) point out that the Leg 180 dolerites have trace element compositions similar to Ontong–Java Plateau basalts, and suggest that they are therefore related to an intraplate magmatism derived from an enriched mantle source. On the other hand, this analogy is not fully supported by previous studies (Jenner, 1981; Davies and Jacques, 1984; Permana, 1998; Monnier et al., 1995, 1999, 2000; Omang and Barber, 1996; Yumul et al., 1997; Tamayo, 2004) as well as by our new geochemical data arguing for a discrete arc-related magma influence. Indeed, the presence of weak Nb and Zr anomalies in most samples (Fig. 4B) likely suggests the contribution of a source linked to a volcanic arc (Fig. 5) (Saunders and Tarney, 1984; Foley et al., 2002; Tamayo, 2004). Slight LILE enrichments (Th and Ta) combined to weak HFSE (Zr and Nb) negative anomalies that are observed in the Mount Moresby dolerites resemble those already documented in the Cyclops–Seram ophiolite (Monnier et al., 1999). The geochemical compositions of dolerites have affinities with part of the ophiolitic sections outcropping in the Papua New Guinea Island as for example the Sentani basalts in the Cyclops ophiolites (Fig. 6 and Table 4). We propose that a discrete influence of a subduction zone recorded in the trace element compositions (Table 4) of Mount Moresby dolerites is compatible with a back-arc setting in agreement with the previous interpretations of Pubellier et al. (2004). Our interpretation is reinforced by the recent evolution of views concerning tectonic settings in which ophiolites formed. Recent studies demonstrate that it is not possible to emplace a true N-MORB derived ophiolite by obduction onto a passive margin instead of fore-arc and back-arc oceanic crust fragments. Stern and Bloomer (1992), Shervais (2001), Stern (2004) argued that, most if not all well preserved ophiolites, formed in suprasubduction zones. This conclusion is supported by the rheological and the geochemical characteristics of the ophiolitic rocks. Indeed, studies on modern and rapid subduction zones (e.g., the Eurasian margin) have demonstrated that such a geotectonic context is favorable to open small oceanic basins giving rise to a succession of marginal basins separated by continental fragments. When such a rapid plate convergence context is associated with oblique convergence, low density

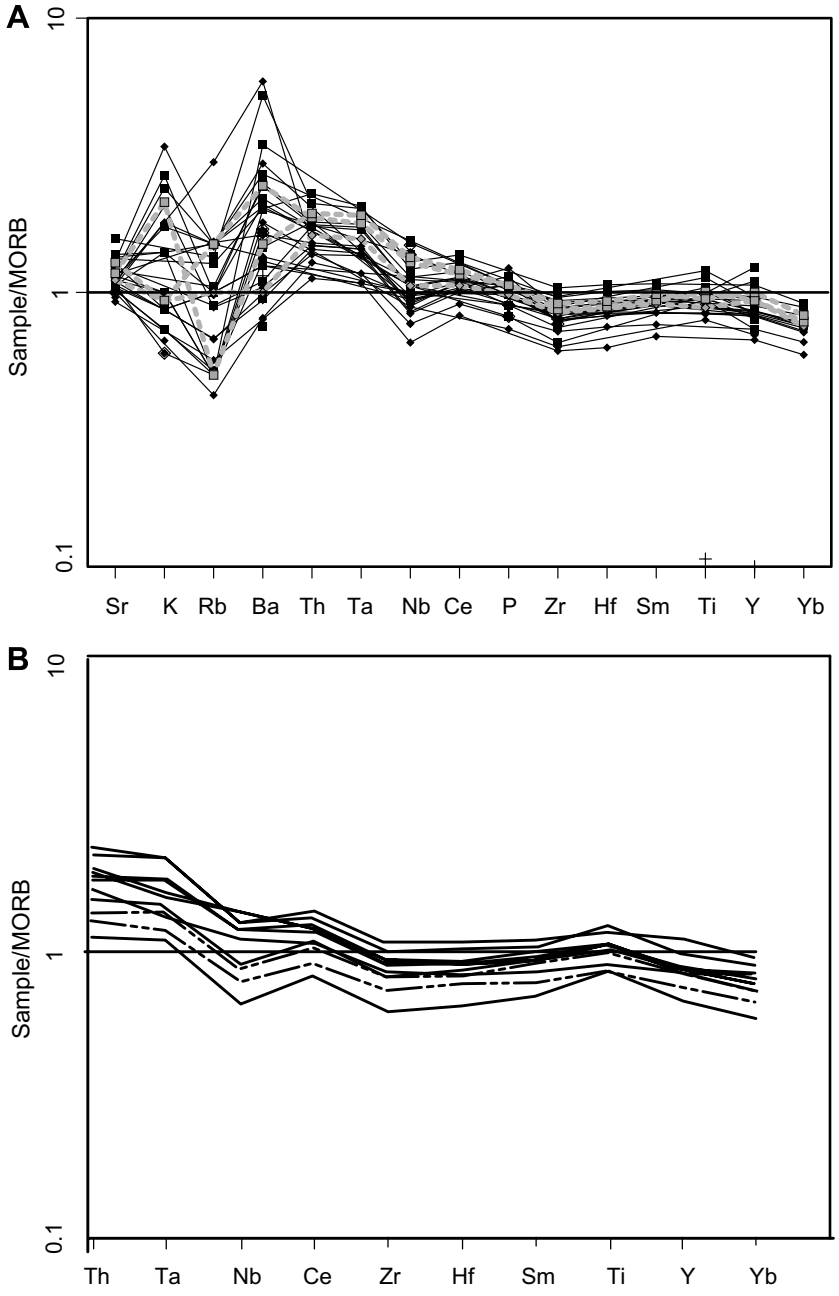

Fig. 4. Multi-element diagrams normalized to MORB (Anderson, 1989) for Leg 180 dolerites. (A) The large scattering in the relative abundance of the most incompatible LILE elements (K, Rb, and Ba) results from hydrothermal alteration of dolerites by seawater. Samples from Brooks and Tegner (2001) are reported as dotted lines. (B) A multi-element diagram built with the most immobile trace elements reveals the homogenous chemical composition of dolerites from Leg 180.

young oceanic crust formed in fore-arc and/or bark-arc settings can be juxtaposed to an old, cold and dense oceanic lithosphere. Sinking of the cold and dense oceanic lithosphere induce the subduction until its total disappearance. The forced subduction of a buoyant continental fragment attached to the oceanic lithosphere leads to failure of the subduction zone, followed by isostatic rebounds of the buoyant crust, itself overlain by the low density young oceanic lithosphere that was obducted onto the continental fragment during convergence (see Fig. 3 in Stern, 2004).

Moreover the suprasubduction zone is recognized as the tectonic setting capable to reconcile the wide range of geochemical signatures (fore-arc, back arc, islands arc and N-MORB) observed in the ophiolitic fragments outcropping on the Papua New Guinea Island.

A method for estimating the composition of the source consists in computing the trace element content of the residue in equilibrium with the basaltic liquid assumed to be represented by the least differentiated sample, the dolerite 49R-3W 80-83, Hole 1109D. The absence of significant heavy REE depletion in the studied rocks suggests that

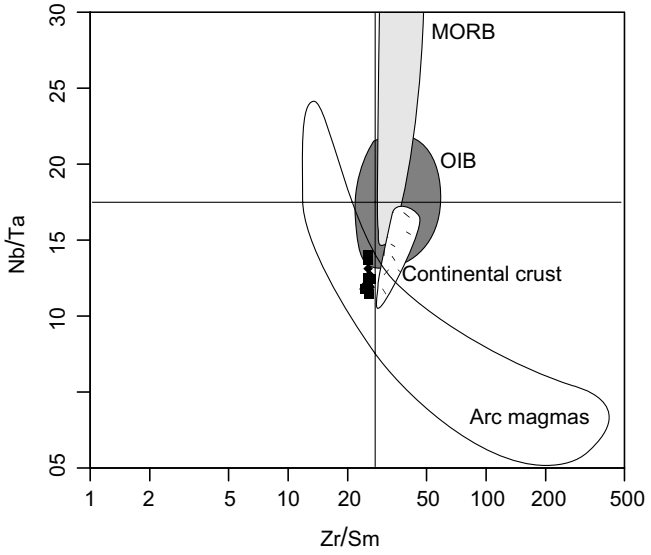

Fig. 5. Nb/Ta vs. Zr/Sm diagram (Foley et al., 2002) that suggests the arc affinity of Leg 180 dolerites. Vertical and horizontal lines illustrate the primitive mantle values according to Sun and McDonough (1989).

the mantle source was most likely a spinel lherzolite rather than a garnet lherzolite. In addition, the flat profile of incompatible elements (Fig. 4A) in the vicinity of Zr (Brooks and Tegner, 2001) suggests a melting rate of the mantle source of at least 10% (Desmurs et al., 2002). Accordingly, we calculated the composition of a garnet-free mantle in equilibrium with 5–30% of melt. This model mantle has a composition comparable to the depleted mantle (Fig. 7) proposed by the GERM project for melting rates higher than 5% (http://earthref.org/GERM/ and Tables 1E and 1D).

One of the most striking geochemical signatures of the Woodlark dolerites is their discrete but systematic negative Nb anomaly (Fig. 4) which is shared by rocks from numerous ophiolite series outcropping in the Papua New Guinea. Accordingly, many authors do not rule out their formation in a suprasubduction zone environment including the fore-arc basin as examplified by the Marum and Cyclops ophiolites (Jenner, 1981; Monnier et al., 2003) and back-arc environments with the PUB (Davies and Jacques, 1980; Jacques and Chapell, 1980).

6. Summary and conclusions

A scenario is proposed to depict the evolution and relationships between the various magmas that generated the dolerites and gabbros constituting the basement of the Moresby Seamount (Fig. 8). The parent magma was generated by at least 10% melting of a spinel lherzolite. Early crystallization of clinopyroxene, spinel and more or less plagioclase took place at a relatively high pressure (7–10 kb) in the mantle. More or less differentiated liquids migrated into

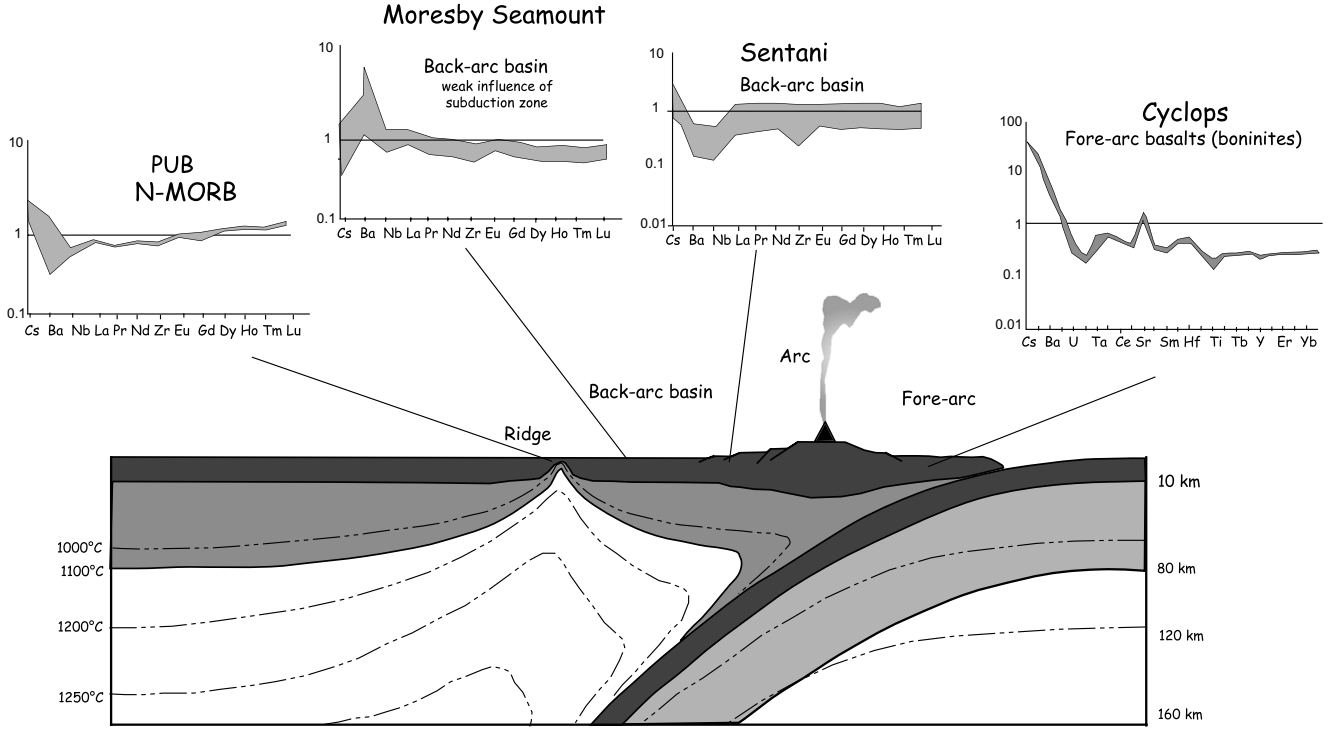

Fig. 6. Sketch of the supra-subduction zone proposed by Pubellier et al. (2004) for the Eastern Indonesia. MORB-normalized multi-element diagrams illustrate the various possible tectonic settings. The PUB is interpreted as mid ocean ridge basalts (Jacques and Chapell, 1980) the Sentani basalts are interpreted as back arc basalts (Monnier et al., 1999) the Cyclops–Seram boninites are interpreted as Island-arc basalts (Monnier et al., 1999). Dolerites from Mount Moresby could have been generated in a mature back-arc basin still under the weak influence of the subduction zone. The multi-element diagrams have been obtained using the values presented in Table 4, normalization is obtained by using MORB composition (in ppm) of Anderson (1989). The compositions used for the diagram of leg 180 dolerites are mentioned in Table 1C and 1E.

Table 4
Selected trace elements (in ppm) analyses of the PUB (Jacques and Chapell, 1980) the Sentani basalts and boninites (Monnier et al., 1999), the MORB composition of Anderson (1989)

Sample	Ormu Boninites			PUB				Sentani			Anderson (1989)
	Cy232b	Cy231	C22	708	706	707	709	Cy26	Cy235	Cy219	MORB
Cs	0.39	0.35	nd	0.017	0.03	0.028	0.015	0.01	0.02	0.04	0.014
Ba	32.94	29.03	34,00	3.99	5.91	14.57	19.05	5.48	2.09	8.06	13.9
Nb	0.51	0.42	0.4	2.04	1.76	1.6	1.63	0.86	0.48	1.71	3.5
La	1.57	1.46	0.8	2.34	2.68	2.71	2.55	2.56	1.44	4.92	3.89
Pr	0.52	0.49	nd	1.28	1.3	1.27	1.26	1.49	0.84	2.75	2.07
Nd	2.54	2.39	1.2	7.47	7.78	7.42	7.66	8.04	4.67	14.98	11.2
Zr	37.97	32.11	19,00	63.2	68.7	64.5	67,00	33.53	24.25	134,00	104,00
Eu	0.3	0.28	0.16	1.01	1.05	0.99	1.04	0.84	0.65	1.66	1.33
Gd	1,00	0.98	0.5	4.28	3.55	3.63	3.53	3.32	2.29	6.36	5.08
Dy	1.21	1.13	0.6	5.45	5.86	5.43	5.65	3.88	2.96	7.86	6.3
Ho	0.26	0.25	nd	1.242	1.328	1.273	1.331	0.82	0.63	1.68	1.34
Tm	0.12	0.11	nd	0.586	0.625	0.566	0.586	0.34	0.28	0.74	0.62
Lu	0.13	0.12	nd	0.62	0.67	0.59	0.65	0.31	0.27	0.75	0.59

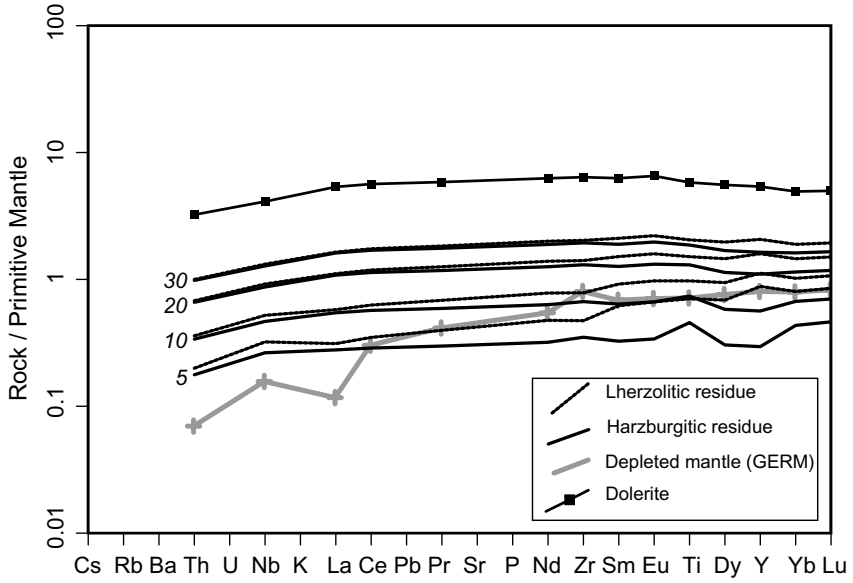

Fig. 7. Primitive mantle-normalized (Sun and McDonough, 1989) multi-element diagrams showing mantle compositions compatible with the genesis of dolerites from the Leg 180. The compositions are calculated by using (1) equilibrium melting equation; (2) partition coefficients from the literature; (3) increasing melt fractions of 5%, 10%, 20%, and 30% and mantle residues of either harzburgitic (black line) or lherzolitic (dotted line) compositions. The dolerite 49R-3W 80-83 from Hole1109D has been selected as representative of one of the less differentiated liquid produced by partial melting; it is illustrated by the black line with filled squares. Numbers indicate the melting fraction values. The modeled mantle source of Woodlark dolerites is compared to the depleted mantle (GERM) illustrated by a grey line with crosses (See Table 1E and 1D for composition).

the crust and generated the dolerites from the sites 1109 and 1118. Then, a second stage of differentiation occurred at lower pressure in the crust along the plagioclase + clinopyroxene + ilmenite eutectic and formed the much differentiated gabbros from the site 1117. Weak but common Nb and Zr negative anomalies in the trace element patterns of dolerites suggest the influence of a subduction zone. This ophiolites fragment could have been formed in a back-arc environment rather than within an oceanic basin, in agreement with the regional tectonic setting in SE Asia dominated by the opening of several small basins.

Mineral abbreviations for figures and tables:

Act	actinolite
Cpx	clinopyroxene
Ep	epidote
Hbl	hornblende
Chl	chlorite
Gt	garnet
Sp	spinel
Pg	plagioclase
Ilm	ilmenite
Zo	zoisite

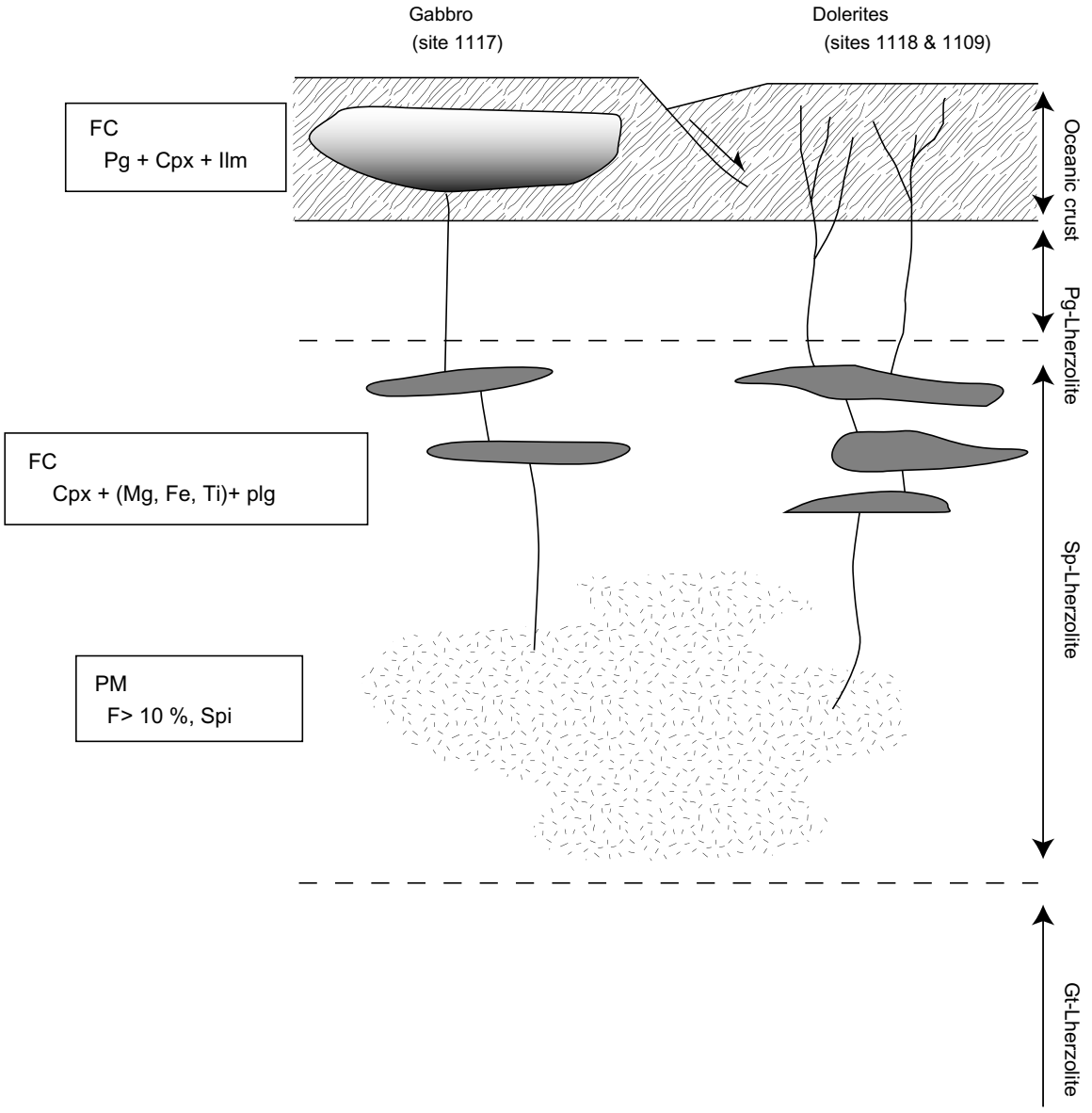

Fig. 8. Schematic drawing corresponding to the model proposed for the petrogenesis of hole 1117 gabbros and holes 1109 and 1118 dolerites. PM: partial melting (F: melting percentage), FC: fractional crystallization.

References

Anderson, D.L., 1989. Theory of the Earth. Blackwell Scientific Publications, Oxford. ISBN: 0-086542-123-4.

Beccaluva, L., Coltorti, M., Giunta, G., Siena, F., 2004. Tethyan vs. cordilleran ophiolites: a reappraisal of distinctive tectono-magmatic features of supra-subduction complexes in relation to the subduction mode. Tectonophysics 393, 163–174.

Belfort, D., 1976. Foramminifera and age of sample from southeastern Papua. Bur. Miner. Resour. Geol. Geophys. Aust. Bull. 165, 73–86.

Brooks, K., Tegner, C., 2001. Affinity of the Leg 180 dolerites of the Woodlark Basin: geochemistry and age. In: Huchon, P., Taylor, B., Klaus, A. (Eds.), Proc. ODP, Sci. Results, 180SR-150.

Bryan, W.B., Finger, L.W., Chayes, F., 1969. Estimating proportions in petrographic mixing equations by least-squares approximation. Science 163, 926–927.

Carignan, J., Hild, P., Mevelle, G., Morel, J., Yeghicheyan, D., 2001. Routine analyses of trace element in geological samples using flow injection and low pressure on-line liquid chromatography coupled to ICP-MS: a study of geochemical reference materials BR, DR-N, UB-N, AN-G and GH, Geostand. Geostandard. Newsl. 25, 187–198.

Davies, H.L., Jacques, A.L., 1984. Emplacement of the ophiolites in Papua New Guinea. In: Gass, I.G., Lippard, S.J., Shelton, A.W. (Eds.), Ophiolites and Oceanic Crust. Blackwell Sci. Pubs., Oxford, pp. 341–349.

Davies, H.L., 1971. Peridotites-gabbro-basalts complex in eastern Papua; an overthrust plate of oceanic mantle and crust. Aust. Bur. Miner. Resour. Geol. Geophys. Bull. 128, 1–48.

Desmurs, L., Müntener, O., Manatschal, G., 2002. Onset of magmatic accretion within a magma-poor rifted margin: a case study from the Platta ocean-continent transition, eastern Switzerland. Contrib. Mineral. Petrol. 144, 365–382.

Foley, S.F., Tiepolo, M., Vannucci, R., 2002. Growth of early continental crust controlled by melting of amphibolite in subduction zones. Nature 417, 637–640.

Gardien, V., LeGall, B., Célérier, B., Louvel, V., Huchon, P., 2001. Low pressure–temperature evolution of the continental crust exhumed during the opening of the Woodlark Basin. In: Huchon, P., Taylor, B., Klaus, A. (Eds.), Proc. ODP, Sci. Results, 180SR-178.

Green, D.H., Ringwood, A.E., 1967. The genesis of basaltic magmas. Contrib. Mineral. Petrol. 15, 103–190.

Jacques, A.L., Chapell, B.W., 1980. Petrology and trace element gochemistry of the Papuan Ultramafic Belt. Contrib. Mineral. Petrol. 75, 55–70.

Jenner, G.A., 1981. Geochemistry of high-Mg andesites from Cape Vogel, Papua New Guinea. Chem. Geol. 33, 307–332.

Lus, Y.W., McDougall, I., Davies, H.L., 2004. Age of the metamorphic ole of the Papuan Ultramafic Belt ophiolites, Papuan New Guinea. Tectonophysics

Martin, H., 1985. Nature, origine et évolution d'un segment de croûte continentale archéenne: contraintes chimiques et isotopiques. Exemple de la Finlande orientale. Mem. CAESS no 1. Rennes, France, pp. 324.

Monnier, C., Girardeau, J., Maury, R.C., Cotten, J., 1995. Back-arc basin origin for the East Sulawesi ophiolites (eastern indonesia). Geology 23, 851–854.

Monnier, C., Girardeau, J., Pubellier, M., Polvé, M., Permana, H., Bellon, H., 1999. Petrology and geochemistry of the Cyclops ophiolite (Irian Jaya, East Indonesia): consequences for the evolution of the north Australian margin during Cainozoic. Mineral. Petrol. 65, 1–28.

Monnier, C., Girardeau, J., Pubellier, M., Permana, H., 2000. L'Ophiolite de la Chaîne Centrale d'Irian Jaya (Indonésie) Evidences pétrologiques et géochimique pour une origine dans un bassin d'arrière arc. C. R. Acad. Sci. Terre Ser. II A 331, 691–699.

Monnier, C., Girardeau, J., Réhault, J.-P., Permana, H., Bellon, H., 2003. Dynamics and age of formation of the Seram–Ambo ophiolites (Central Indonesia). Bull. Soc. Géol. (France) 174, 529–543.

Monteleone, B., Baldwin, S., Ireland, T., Fitzgerald, P., 2001. Thermochronologic constraints for the tectonic evolution of the Moresby Seamount, Woodlark Basin, Papua New Guinea. In: Huchon, P., Taylor, B., Klaus, A. (Eds.), Proc. ODP, Sci. Results, 180SR-173.

Moyen, J.-F., Martin, H., Jayananda, M., 2001. The Closepet granite (S. India) multi-elements geochemical modelling of Crust–Mantle interactions during late-Archaean crustal growth. Precambrian Res. 112, 87–105.

Omang, S.A.K., Barber, A.J., 1996. Origin and tectonic significance of metamorphic rocks associated with the Darvel Bay Ophiolite, Sabah, Malesia. In: Hall, R., Blundell, D. (Eds.), Tecotnic Evolution of the SE Asia, vol. 106. Spe. Pub. Geol. Soc., London, pp. 263–279.

Permana, H., 1998. Dynamique de la mise en place des ophiolites d'Irian Jaya (Indonésie). PhD Thesis of the University of Nantes, pp. 314.

Pubellier, M., Monnier, C., Maury, R., Tamayo, R., 2004. Plate kinematics, origin and tectonic emplacement of supra-subduction ophilites in SE Asia. Tectonophysics 392, 9–36.

Rollinson, H., 1993. Using Geochemical Data. Longman, London, pp. 352.

Saunders, A.D., Tarney, J., 1984. Geochemical characteristics of basalts volcanism within back-arc basin. In: Kokelaar, B.P., Howell, M.F. (Eds.), Marginal Basins Geology: Volcanism and Associated Sedimentary and Tectonics Processes in Modern and Ancient Marginal Basins. BlackWell Scientific Publication, Geological Society, London, pp. 57–76.

Shervais, J.W., 2001. Birth, death and resurrection: the life cycle of suprasubduction zone ophiolites, Geochém. Geophys. Geosyst. 2, (paper 2000GC000080).

Smith, I.E., Davies, H.L., 1976. Geology of the southeastern Papuan Mainland. Bur. Miner. Resour. Geol. Geophys. Aust. Bull. 165, 109.

Stern, R.J., Bloomer, S.H., 1992. Subduction zone infancy: examples from the Eocene Izu–Bonin–Mariana and Jurassic California. Geol. Soc. Am. Bull. 104, 1621–1636.

Stern, R.J., 2004. Subduction initiation: spontaneous and induced. Earth Planet. Sci. Lett. 226, 275–292.

Sun, S.S., McDonough, W.F., 1989. Chemical and isotopic systematics of oceanic basalts: implications for mantle composition and processes. In: Saunders, A.D., Norry, M.J., (Eds.), Magmatism in ocean basin, pp. 313–345.

Tamayo, R., Maury Yumul Polvé, M., Cotton, J., Dimantala, C.B., Olaguera, F.O., 2004. The early geodynamic evolution of the Philippine Archipelago: constraints from geochemistry of the ophiolitic complexes, Spec. Publ. Bull. Soc. Géol. France.

Taylor, B., Huchon, P., Klaus, A., et al., 1999. Proc. ODP., Init. Repts. 180. Ocean Drilling Program, Texas A& M University, College Station. TX 77845-9547, USA.

Yumul, G.P., Balce, G.R., Dimatala, C.B., Datuin, R.T., 1997. Distribution, geochemistry and mineralization potential of Philippin ophiolite and ophiolitic sequence. Ofioliti 22, 47–56.